Journal of Materials Chemistry A

Accepted Manuscript

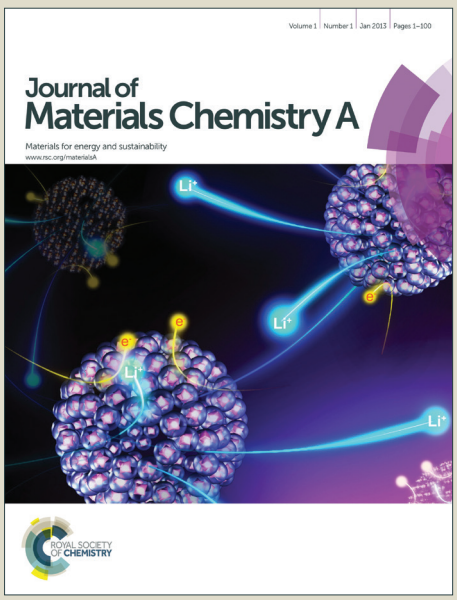

ROYAL SOCIETY OF CHEMISTRY

www.rsc.org/materialsA

High performance perovskite-sensitized nanoporous titanium dioxide photoanodes by in situ method for use in perovskite solar cells

Yaoming Xiao[*], *Gaoyi Han*[*], *Yanping Li, Miaoyu Li and Yunzhen Chang*

Perovskite-sensitized nanoporous TiO_2 photoanode with several micrometers of the thickness, was firstly prepared by an in situ technique. The excellent contacting between the TiO_2 and perovskite could be beneficial to the separation and transmission of the electron and hole, the sufficient filling and abundant $CH_3NH_3PbI_3$ could enhance the absorption and utilization of sunlight, finally obtaining an efficient perovskite solar cell. 10.03% of the cell efficiency was acquired without adding hole transporting material into the device.

Keywords: in situ method, perovskite, titanium dioxide, photoanode, solar cell

Introduction

In 1991, M. Grätzel and his co-worker reported a novel dye-sensitized solar cell (DSC) that rapidly attracted extensive attention due to its low cost, environmental friendliness, and relatively high energy conversion efficiency.[1-3] And in 2014, 13% of the DSC efficiency was received

[*] Dr. Y. M. Xiao, Prof. G. Y. Han, Dr. M. Y. Li, Dr. Y. P. Li, Dr. Y. Z. Chang

Institute of Molecular Science, Shanxi University, Taiyuan 030006, P. R. China.

Tel: +86 351 7010699; Fax: +86 351 7016358

E-mail: ymxiao@sxu.edu.cn (Yaoming Xiao); han_gaoyis@sxu.edu.cn (Gaoyi Han)

based on a porphyrin sensitizer and cobalt (II/III) redox electrolyte.[3] Recently, a new class of hybrid organic-inorganic perovskite compounds ($CH_3NH_3PbX_3$, X = I, Br, and Cl) replace the traditional dye (N719) as light harvesters for solar cells due to their direct band gap, wide light-absorption, and high carrier mobility.[4-10] The perovskite solar cell (PSC) shows an impressive high open circuit voltage and realizes an all-solid-state solar cell by replacing the liquid electrolyte with a hole transporting material (HTM) for the production and stability of the photovoltaic device.[11,12]

There are two major technologies for the preparation of PSCs. On the one hand, one-step[5,7,13-17] or two-step[4] solution process was used to prepare the perovskite sensitizer in the TiO_2 film. As a result, two-step method could obtain higher performance PSC than that of the one-step method due to its more controllable perovskite sensitizer of size. Recently, Xiao et al. report on an interdiffusion method to fabricate pin-hole free perovskite films using a low temperature solution process, and a high efficiency of 15.4% was achieved for the devices under one sun illumination.[18] However, the mesoporous TiO_2 photoanode with hundreds of nanometers of the thickness, is an important factor for the solution process to match with the preparation of perovskites, and the perovskite is hard to fill into the TiO_2 film.[14-16] On the other hand, in 2013, Prof. Snaith reported an efficiency of 15.4% perovskite solar cells by vapour deposition.[7] This method could win smaller and more homogeneous $CH_3NH_3PbI_3$ film. However, the $CH_3NH_3PbI_3$ film was only formed on the surface of the TiO_2 with a planar structure, the thickness of the TiO_2 film should be thinner than the electron diffusion length of the $CH_3NH_3PbI_3$ to realize the separation of the electron and hole. The planar structure could lead to a waste of the intrinsic and high surface area of the TiO_2 nanoparticles.

Therefore, here we report on an in situ preparation of perovskite-sensitized nanoporous TiO_2

photoanode with several micrometers of the thickness for the PSC. Firstly, a lead compound (such as lead iodide, lead acetate, lead nitrate, and lead oxide) is homo-dispersed into the TiO_2 colloid, and then spin-coated on the dense blocking TiO_2 layer, after sintering, TiO_2&PbO composite film is obtained. Secondly, the TiO_2&PbO composite film is dipped in a HI acid solution, after full reaction and drying, the TiO_2&PbI_2 composite film is achieved. Finally, the TiO_2&PbI_2 composite film is soaked in a solution of CH_3NH_3I and rinsed with isopropyl alcohol, after drying, the perovskite-sensitized nanoporous TiO_2 photoanode (TiO_2&$CH_3NH_3PbI_3$ composite film) is gained by the in situ method. Comparing to the pervious results, the in situ method allows a better contacting between the TiO_2 and perovskite, which is beneficial to the separation and transmission of the electron and hole, reducing the demand of the TiO_2 thickness; better filling of the perovskite into the TiO_2 film, which can enhance the absorption of sunlight; and thicker photoanode to use the advantage on the surface area of the TiO_2 nanoparticles and to absorb more sunlight to possess a higher photovoltaic performance. Furthermore, a supplementary perovskite on the in situ photoanode by the two-step method could further enhance the photovoltaic performance of the PSC. **Figure 1** shows a schematic diagram of preparation processes for the three kinds of PSCs prepared by two-step, in situ, and in situ with two-step methods, respectively.

Experimental

Materials

Acetone, isopropyl alcohol, methanol, ether, hydroiodic acid (45 wt.% in water), methylamine (30% in methanol), lead iodide (PbI_2), N,N-dimethylformamide (DMF), tetrabutyl titanate, and Triton X-100 were purchased from Shanghai Chemical Agent Ltd., China (Analysis

purity grade). The above agents were used without further purification. The CH_3NH_3I was prepared by reacting 20 mL hydroiodic acid (45 wt.% in water) and 20 mL methylamine (30% in methanol) in a 250 ml round-bottomed flask at 0 °C for 2 h with stirring. Then the resulting solution was evaporated at 50 °C for 1 h. The precipitate was washed three times with diethyl ether, dried at 60 °C under a vacuum oven for 24 h, and used without further purification.

Two-step preparation of the photoanode

The two-step preparation of the photoanode was carried out according to the reported procedure.[4] A layer of dense blocking TiO_2 (bl-TiO_2) was coated onto a FTO substrate by spin-coating of 3 mM tetrabutyl titanate in isopropyl alcohol with a small quantity of Triton X-100 at 500 r.p.m. for 10 s then at 6,000 r.p.m. for 30 s, then heat-treated at 450 °C for 30 min. The nanoporous TiO_2 (np-TiO_2) film was spin-coated on the bl-TiO_2 substrate under the same coating parameters using the TiO_2 colloid, which was prepared according to our previous reports.[19-21] The film was calcined again at 450 °C for 30 min, thereby the TiO_2 film was gained. Then spin-coating a PbI_2 solution in DMF (462 mg·mL^{-1}) on the TiO_2 film. After drying, the film was dipped in a solution of CH_3NH_3I in isopropyl alcohol (10 mg·mL^{-1}) for 20 s and rinsed with isopropyl alcohol. After drying, the TiO_2&$CH_3NH_3PbI_3$ composite film by the two-step method was gained.

In situ preparation of the photoanode

PbI_2 solution in DMF was added to the aforementioned TiO_2 colloid with an atomic ratio of Pb : Ti = 1 : 2. After stirring, The mixed colloid was spin-coated on the aforementioned bl-TiO_2 substrate under the same coating parameters, then heat-treated at 450 °C for 30 min. After cool to room temperature, the TiO_2&PbO composite film was dipped in a HI solution (0.5 mol·L^{-1}) to form TiO_2&PbI_2 composite film. After drying, the TiO_2&PbI_2 composite film was dipped in a

solution of CH_3NH_3I in isopropyl alcohol (10 mg·mL^{-1}) for 20 s and rinsed with isopropyl alcohol. After drying, the TiO_2&$CH_3NH_3PbI_3$ composite film by the in situ method was obtained.

In situ with two-step photoanode was prepared as fellow: the PbI_2 solution in DMF was spin-coated on the aforementioned TiO_2&PbI_2 composite film, after drying, the film was dipped in a solution of CH_3NH_3I in isopropyl alcohol (10 mg·mL^{-1}) for 20 s and rinsed with isopropyl alcohol. After drying, the TiO_2&$CH_3NH_3PbI_3$ composite film by the in situ with two-step method was achieved.

Solar cell fabrication

Gold (80 nm) was sputtered on top of the TiO_2&$CH_3NH_3PbI_3$ composite film to form the back contact by using a magnetron sputtering equipment (ETD-2000M, Beijing Elaborate Technology Development Ltd., China) to fabricate the PSC. The PSCs based on TiO_2&$CH_3NH_3PbI_3$ composite films by two-step, in situ, and in situ with two-step methods, were described as PSC-a, PSC-b, and PSC-c, respectively.

Characterizations and measurements

The surface morphologies of the photoanodes were observed using a scanning electron microscopy (SEM, JEOL-JSM-6701F) operating at 10 kV. The phase identification of the product was conducted with powder X-ray diffraction (XRD, BRUKER D8-ADVANCE), by which the product powder was compacted on the plastic substrate attached to the XRD, and the powder was collected together from the FTO glass and following a grinding process. Ultraviolet to visible (UV-Vis) reflectance and absorbance spectra of the samples were performed with an Agilent 8453 UV-Vis diode array spectrophotometer.

The electrochemical impedance spectroscopy (EIS) of the PSC was performed using a CHI660D (Shanghai Chenhua Device Company, China) electrochemical measurement system at

a constant temperature of 20 °C in ambient atmosphere under illumination by a solar simulator (CEL-S500, Beijing Ceaulight Science and Technology Ltd., China), and the impedance data covered a frequency range of 1-10^5 Hz with 5 mV of amplitude and zero bias potential. The resultant impedance spectra were simulated using the Z-view software. The incident monochromatic photon-to-current conversion efficiency (IPCE) curves were measured with a solar cell QE/IPCE measurement system (Solar Cell Scan 100, Beijing Zolix Instruments Co. Ltd., China). The photocurrent density-voltage (*J-V*) characteristic of the PSC was carried out using a computer-controlled CHI660D in ambient atmosphere. The incident light intensity was set under 100 mW·cm^{-2} (AM 1.5), and a black mask (0.50 cm^2) was used on top of the device to control the active cell area for the light irradiation.

Results and discussion

The phase identification of the products during the in situ preparation process was conducted with the powder X-ray diffraction (XRD). **Figure 2** (1) demonstrates the XRD pattern of the TiO_2&PbO composite film. Characteristic diffraction peak at 2θ of 25.3º for titania anatase (101) crystal face is observed, and all sharp peaks can be indexed as titania anatase (Joint Committee on Powder Diffraction Standards (JCPDS) card no. 21-1272). Whereas, the characteristic diffraction patterns at 28.5, 31.8, 36.1, 50.9, and 56.7 º are from the PbO (corresponding to the data in JCPDS card no. 78-1666), which was converted from the starting material of PbI_2 after the sintering process. After the HI treatment, the PbO component in the TiO_2&PbO composite film was re-generated to PbI_2. The crystalline phase of PbI_2 can be observed at 12.6, 25.7, 34.0, 39.5, and 52.3 º, which are identified to be the (001), (002), (102), (003), and (004) diffraction signals, respectively, according to the JCPDS card no. 73-1750. However, the TiO_2 component

was retained. After soaking in the CH_3NH_3I solution, the PbI_2 was changed to $CH_3NH_3PbI_3$. Strong diffraction peaks are observed at approximately 14.2, 20.0, 23.6, 24.6, 28.5, 31.9, 35.0, 40.6, and 43.2°, respectively corresponding to the reflections from (110), (112), (211), (202), (220), (310), (312), (224), and (314) crystal planes of the tetragonal perovskite structure.[22] And the characteristic diffraction peaks of the TiO_2 are weakened due to the TiO_2 was covered with the $CH_3NH_3PbI_3$. The XRD patterns indicate that the perovskite sensitized TiO_2 (TiO_2&$CH_3NH_3PbI_3$ composite film) was successfully prepared onto the surface of FTO glass substrate. Inset of **Figure 2** is the real photographs of the three products, the color was changed from white to yellow and finally to black.

In order to make a comparison, two-step method was selected to prepare the photoanode according to the reported procedure.[4] **Figure 3** a-1, a-2, and a-3 show the top-view and cross-sectional SEM images of the photoanode prepared by the two-step method. It can be found that the $CH_3NH_3PbI_3$ film was only formed on the surface of the nanoporous TiO_2, it was hard to fill into the nanoporous TiO_2 film, and the thickness of the TiO_2 film was about 5.2 μm. The $CH_3NH_3PbI_3$ has a diffusion length of 129 ± 41 nm for electrons,[10] which requests that the thickness of the TiO_2 films should be thinner than the electron diffusion length. Therefore the 5.2 μm thickness of the TiO_2 film would hinder the electron transporting from the $CH_3NH_3PbI_3$ film to the FTO glass, which could remarkably reduce the PSC performance. Decreasing the thickness of the TiO_2 film is an important method to accord with the electron diffusion length of the $CH_3NH_3PbI_3$. However, the advantage on the surface area of the TiO_2 nanoparticles can not be fully utilized. **Figure 3** b-1, b-2, and b-3 show the top-view and cross-sectional SEM images of the photoanode based on the in situ method. The nanoporous TiO_2 film was well filled and contacted with the $CH_3NH_3PbI_3$, which is beneficial to the separation and transmission of the

electron and hole, resulting in a very thick TiO_2 film could work in the PSC. The thickness of the TiO_2 film was about 6.0 μm, which could use the advantage on the surface area of the TiO_2 nanoparticles, leading to a high sunlight absorption and a high photovoltaic performance. However, there are some TiO_2 nanoparticles reveal out of the surface of the TiO_2 film, which will directly contact with the Au electrode by the subsequent solar cell fabrication, resulting in an unwished increase of the electron recombination. For this consideration, introduction of the $CH_3NH_3PbI_3$ film on the surface of the TiO_2 film, would further influence the performance of the PSC. The $CH_3NH_3PbI_3$ was well-contacted with the TiO_2 and well-filled into the photoanode, and also well-covered on the surface of the TiO_2 film (**Figure 3** c-1, c-2, and c-3), which was prepared by the in situ method firstly and then two-step method.

Figure 4 compares the UV-Vis reflectance and absorption spectra of the photoanodes by two-step, in situ, and in situ with two-step methods, respectively. From the **Figure 4** (a), the reflectance of the two-step sample is the highest, the lower one is the in situ sample, and the smallest one is the sample by the in situ with two-step method. One possible explanation is that more $CH_3NH_3PbI_3$ was filled into the photoanode to absorb more sunlight, and the $CH_3NH_3PbI_3$ on the TiO_2 surface could further absorb sunlight. Therefore, the photoanode by the in situ with two-step method shows a lowest reflectance. And the other reason is that the nanoporous TiO_2 film has a strong optic scattering effect, which leads to the low reflectance. The lower reflectance means that less light is reflected off the space and more light is utilized. UV-Vis absorption spectra further confirms the conclusions of the UV-Vis reflectance. The photoanode by the in situ with two-step method presents the highest UV-Vis absorption among the three photoanodes.

Gold (80 nm) was sputtered on top of the perovskite-sensitized nanoporous TiO_2 photoanode to form the back contact by using a magnetron sputtering equipment to fabricate the PSC. It

should be noted that the hole transporting material was absent in these PSCs. Electrochemical impedance spectroscopy (EIS) for the PSC was used to characterize the internal resistance and charge transfer kinetics of the solar cell,[23] as shown in **Figure 5**. The EIS was performed under illumination with an incident light intensity of 100 $mW \cdot cm^{-2}$ (AM 1.5) by a solar simulator, and the impedance data covered a frequency range of 1-10^5 Hz with 5 mV of amplitude and zero bias potential. The equivalent circuit of this model (inset of **Figure 5** a) has been already reported.[21,24,25] The intercept of the real axis at high frequency is the ohmic series resistance (R_S) including the sheet resistance of the TiO_2 photoanode and the $CH_3NH_3PbI_3$ resistance. The first semicircle at high frequency refers to the R_1 for the charge-transfer resistance at the Au/$CH_3NH_3PbI_3$ interface, while the second semicircle at middle frequency refers to the R_2 for the charge-transfer resistance at the $CH_3NH_3PbI_3/TiO_2$ interface.[21,24,25] The constant phase elements (C_1 and C_2) are frequently used as substitutes for the capacitors in an equivalent circuit to fit the impedance behavior of the electrical double layer more accurately while the double layer does not behave as an ideal capacitor.[21,24,25]

The results of the impedance data are shown in **Table 1**. The R_S, R_1, and R_2 values of the PSC-c under AM 1.5 illumination are 9.59, 1.25, and 9.74 $\Omega \cdot cm^2$, respectively, which are the lowest values among the three kinds of devices, owing to the high carrier mobility of the $CH_3NH_3PbI_3$ was well contacted and filled up in the TiO_2 film, and the well contacting between the TiO_2 and perovskite leaded to a beneficial to the separation and transmission of the electron and hole. The lower resistances could result in a more effective and rapid transporting ability for the electron and hole under illumination, which would further improve the performance of the PSC especially the fill factor. In addition, a larger C_2 of the PSC-c corresponds to its larger surface area of the photoanode, which can enhance the photovoltaic properties especially the

photocurrent. Based on the EIS model, the effective electron lifetime for recombination (τ_r) in the photoanode can be calculated from the minimum angular frequency (ω_{min}) value by the following equation: $\tau_r = 1 / \omega_{min}$, where the ω_{min} values come from the impedance semicircle at middle frequencies in the Bode spectrum. The τ_r value for the device of PSC-a has a highest value of 17.78 ms, this is due to the lowest carrier mobility in the TiO_2 photoanode. While the τ_r values for the PSC-b and PSC-c are 6.83 and 4.66 ms, this may be owing to the high carrier mobility of the $CH_3NH_3PbI_3$ in the TiO_2 for the reduced effective electron lifetime. The lower τ_r value could increase the electron recombination, resulting in a depressed cell performance.[21,26-28] However, the photon-generated electrons from the excited perovskite $CH_3NH_3PbI_3$ can be quickly separated and transfered to the conductive band of semiconductor TiO_2 in the level of femtosecond, therefore the 4.66 ms can provide enough time for the carrier transport.[21,29]

The incident monochromatic photon-to-current conversion efficiency (IPCE) of the three kinds of PSCs were characterized and are shown in **Figure 6** a, which reflects the light response of the PSC and is directly related to the short-circuit current density (J_{SC}). All the PSCs show a wide light response from 350 nm to higher than 750 nm, with the maximum at ca. 500 nm. The IPCE over 650 nm is lower then what has been reported in many literatures, this might be owing to the micrometers thickness of the TiO_2 film by the in situ method, which is much thicker than the hundreds of nanometers of TiO_2 layer by conventional solution processes or vapour deposition. The IPCE of the PSC-c is the highest one among the three kinds of PSCs, due to that more $CH_3NH_3PbI_3$ was filled into the TiO_2 to absorb and utilize more sunlight, the well contact between the TiO_2 and perovskite resulted in a quick and efficient separation and transmission of the electron and hole, and the $CH_3NH_3PbI_3$ on the TiO_2 surface could further enhance the sunlight absorption and decrease the electron recombination. These results were in agreement

with the UV-Vis absorption spectra, EIS tests, and following *J-V* measurements.

The photovoltaic properties of PSCs were measured under full sunlight illumination (100 $mW \cdot cm^{-2}$, AM1.5 G), which were retested many times without obvious change, and the results were summarized in **Table 2**. The device parameters show smaller deviation then what has been reported in the literature,[30] this might be due to that more uniform perovskite loading in the thicker TiO_2 film compared to that of prepared by conventional solution processes or vapour deposition. As can be seen in **Figure 6** b, the PSC-a produces a cell efficiency of 3.35%, owing to the thickness of the TiO_2 film (5.2 μm) is much thicker than the electron diffusion length of the $CH_3NH_3PbI_3$ (about 130 nm), which hindered the electron transporting from the $CH_3NH_3PbI_3$ film to the FTO glass, and then remarkably reduced the PSC performance. It is obvious that the photovoltaic performances of the PSC-b became much better while the preparation method was switched from two-step mode to in situ mode. As can be found in **Figure 6** b, the J_{SC}, open-circuit voltage (V_{OC}), and fill factor (*FF*) values of the PSC-b are observably increased due to the $CH_3NH_3PbI_3$ well contacted and filled into the nanoporous TiO_2 film, leading to the decreased values of the R_S, R_1, and R_2.[31,32] The photovoltaic performance the PSC-c is further enhanced by employing an additional $CH_3NH_3PbI_3$ film on the top of the in situ photoanode, attributing to the $CH_3NH_3PbI_3$ on the TiO_2 surface could further improve the sunlight absorption and decrease the electron recombination. As a result, the PSC-c demonstrates a highest J_{SC} value of 17.56 $mA \cdot cm^{-2}$, V_{OC} of 0.84 V, *FF* of 0.68, and supplies a cell efficiency of 10.03%, even though the hole transporting material is absent in the PSC.

Conclusions

In summary, an in situ method was firstly employed to prepare perovskite-sensitized

nanoporous TiO_2 photoanode for the PSC. Because of the excellent contacting between the TiO_2 and perovskite, and sufficient filling of the perovskite into the TiO_2 film, the as-prepared photoanode could be much thicker than that of prepared by conventional solution processes or vapour deposition. These results could observably enhance the absorption of sunlight due to taking full advantage of the high surface area of the TiO_2 nanoparticles, and much more $CH_3NH_3PbI_3$ to absorb sunlight. Moreover, the excellent contacting between the TiO_2 and perovskite could be beneficial to the separation and transmission of the electron and hole, obtaining an efficient perovskite solar cell. Furthermore, a supplementary perovskite on the in situ photoanode by the two-step method could further enhance the photovoltaic performance of the PSC, 10.03% of the cell efficiency was acquired. Studying on devices with variable thickness of TiO_2, changing the organometallic three halide perovskite to mixed halide perovskite, and adding hole transporting material into the device, may be informative to further increase the cell efficiency based on the in situ method.

Acknowledgments

The authors appreciate funding from National Natural Science Foundation of China (21274082 and 21073115) and Shanxi Province (2012021021-3), the Program for New Century Excellent Talents in University (NCET-10-0926), Scientific and Technologial Innovation Programs of Higher Education Institutions in Shanxi, and the Scientific Research Start-up Funds of Shanxi University (020351801003).

References

1 B. O' Regan, M. Grätzel, *Nature* **1991**, *353*, 737.

2 A. Yella, H. Lee, H. Tsao, C. Yi, A. Chandiran, M. Nazeeruddin, E. Diau, C. Yeh, S. Zakeeruddin, M. Grätzel, *Science* **2011**, *334*, 629.

3 S. Mathew, A. Yella, P. Gao, R. Humphry-Baker, B.Curchod, N. Ashari-Astani, I. Tavernelli, U. Rothlisberger, M. Nazeeruddin, M. Grätzel, *Nature Chem.* **2014**, *6*, 242.

4 J. Burschka, N. Pellet, S. Moon, R. Humphry-Baker, P. Gao, M. Nazeeruddin, M. Grätzel, *Nature* **2013**, *499*, 316.

5 J. Heo, S. Im, J. Noh, T. Mandal, C. Lim, J. Chang, Y. Lee, H. Kim, A. Sarkar, M. Nazeeruddin, M. Grätzel, S. Seok, *Nature Photon.* **2013**, *7*, 486.

6 M. Liu, M. Johnston, H. Snaith, *Nature* **2013**, *501*, 395.

7 M. Lee, J. Teuscher, T. Miyasaka, T. Murakami, H. Snaith, *Science* **2012**, *338*, 643.

8 H. Kim, I. Mora-Sero, V. Gonzalez-Pedro, F. Fabregat-Santiago, E. Juarez-Perez, N. Park, J. Bisquert, *Nature Commun.* **2013**, *4*, 2242.

9 S. Stranks, G. Eperon, G. Grancini, C. Menelaou, M. Alcocer, T. Leijtens, L. Herz, A. Petrozza, H. Snaith, *Science* **2013**, *342*, 341.

10 M. He, D. Zheng, M. Wang, C. Lin, Z. Lin, *J. Mater. Chem. A* **2014**, *2*, 5994.

11 E. Edri, S. Kirmayer, D. Cahen, G. Hodes, *J. Chem. Phys. Lett.* **2013**, *4*, 897.

12 J. Qiu, Y. Qiu, K. Yan, M. Zhong, C. Mu, H. Yan, S. Yang, *Nanoscale* **2013**, *5*, 3245.

13 D. Liu, T. Kelly, *Nature Photon.* **2014**, *8*, 133.

14 A. Dualeh, N. Tétreault, T. Moehl, P. Gao, M, Nazeeruddin, M. Grätzel, *Adv. Funct. Mater.* **2014**, *24*, 3250.

15 G. Eperon, V. Burlakov, P. Docampo, A. Goriely, H. Snaith, *Adv. Funct. Mater.* **2014**, *24*, 151.

16 K. Wojciechowski, M. Saliba, T. Leijtens, A. Abate, H. Snaith, *Energy Environ. Sci.* **2014**,

7, 1142.

17 W. Laban, L. Etgar, *Energy Environ. Sci.* **2013**, *6*, 3249.

18 Z. Xiao, C. Bi, Y. Shao, Q. Dong, Q. Wang, Y. Yuan, C. Wang, Y. Gao, J. Huang, *Energy Environ. Sci.* 2014, DOI: 10.1039/c4ee01138d.

19 J. Wu, Z. Lan, J. M Lin, M. Huang, S. Hao, T. Sato, S. Yin, *Adv. Mater.* **2007**, *19*, 4006.

20 J. Wu, Y. Xiao, G. Yue, Q. Tang, J. Lin, M. Huang, Y. Huang, L. Fan, Z. Lan, S. Yin, T. Sato, *Adv. Mater.* **2012**, *24*, 1884.

21 Y. Xiao, G. Han, Y. Chang, H. Zhou, M. Li, Y. Li, *J. Power Sources* **2014**, 267, 1-8.

22 Y. Zhao, K. Zhu, *J. Phys. Chem. Lett.* **2013**, *4*, 2880.

23 Y. Zhao, J. Zhai, J. He, X. Chen, L. Chen, L. Zhang, Y. Tian, L. Jiang, D. Zhu, *Chem. Mater.* **2008**, *20*, 6022.

24 H. Kim, J. Lee, N. Yantara, P. Boix, S. Kulkarni, S. Mhaisalkar, M. Grätzel, N. Park, *Nano Lett.* **2013**, *13*, 2412.

25 G. Niu, W. Li, F. Meng, L. Wang, H. Dong, Y. Qiu, *J. Mater. Chem. A* **2014**, *2*, 705.

26 J. Kim, J. Koh, B. Kim, S. Ahn, H. Ahn, D. Ryu, J. Kim, E. Kim, *Adv. Funct. Mater.* **2011**, *21*, 4633.

27 J. Koh, J. Kim, B. Kim, J. Kim, E. Kim, *Adv. Mater.* **2011**, *23*, 1641.

28 L. Heng, X. Wang, N. Yang, J. Zhai, M. Wan, L. Jiang, *Adv. Funct. Mater.* **2010**, *20*, 266.

29 S. Ito, Y. Makri, J. Kitamura, *J. Mater. Chem.* **2004**, *14*, 385.

30 J. Wang, J. Ball, E. Barea, A. Abate, J. Alexander-Webber, J. Huang, M. Saliba, I. Mora-Sero, J. Bisquert, H. Snaith, R. Nicholas, *Nano Lett.* **2014**, *14*, 724.

31 G. Mor, K. Shankar, M. Paulose, O. Varghese, C. Grimes, *Nano Lett.* **2006**, *6*, 215.

32 E. Ramasamy, W. Lee, D. Lee, J. Song, *J. Power Sources* **2007**, *165*, 446.

Figure and Table Captions

Table 1 EIS results of the PSC-a, PSC-b, and PSC-c, respectively.

Table 2 The photovoltaic performance of the PSC-a, PSC-b, and PSC-c, respectively.

Figure 1 Schematic diagram of preparation processes for the three kinds of PSCs prepared by two-step, in situ, and in situ with two-step methods, respectively.

Figure 2 XRD patterns of the products in the in situ preparation process; Inset is the real photographs of the three products.

Figure 3 Top-view SEM images of the photoanodes by (a-1) two-step, (b-1) in situ, and (c-1) in situ with two-step methods, respectively; Cross-sectional SEM images of the photoanodes by (a-2, a-3) two-step, (b-2, b-3) in situ, and (c-2, c-3) in situ with two-step methods, respectively.

Figure 4 UV-Vis (a) Reflectance and (b) Adsorption spectra of the photoanodes by two-step, in situ, and in situ with two-step methods, respectively.

Figure 5 (a) Nyquist plots and (b) Bode phase plots of the PSC-a, PSC-b, and PSC-c, respectively; Inset (a) is the equivalent circuit of the PSC.

Figure 6 (a) IPCE and (b) Photocurrent density-voltage characteristics of the PSC-a, PSC-b, and PSC-c, respectively.

Table 1 EIS results of the PSC-a, PSC-b, and PSC-c, respectively.

PSC	R_S ($\Omega \cdot cm^2$)	R_1 ($\Omega \cdot cm^2$)	R_2 ($\Omega \cdot cm^2$)	C_1 ($mF \cdot cm^{-2}$)	C_2 ($mF \cdot cm^{-2}$)	ω_{min} (Hz)	τ_r (ms)
(a)	15.28	2.15	13.67	0.65	0.78	56.23	17.78
(b)	10.87	1.49	9.96	0.76	0.87	146.5	6.83
(c)	9.59	1.25	9.74	0.79	0.93	214.8	4.66

Table 2 The photovoltaic performance of the PSC-a, PSC-b, and PSC-c, respectively.

PSC	J_{SC} (mA·cm^{-2})	V_{OC} (V)	*FF*	η (%)
(a)	9.25 ± 0.04	0.74 ± 0.02	0.49 ± 0.02	3.35 ± 0.03
(b)	15.22 ± 0.05	0.83 ± 0.03	0.64 ± 0.02	8.08 ± 0.04
(c)	17.56 ± 0.06	0.84 ± 0.03	0.68 ± 0.03	10.03 ± 0.06

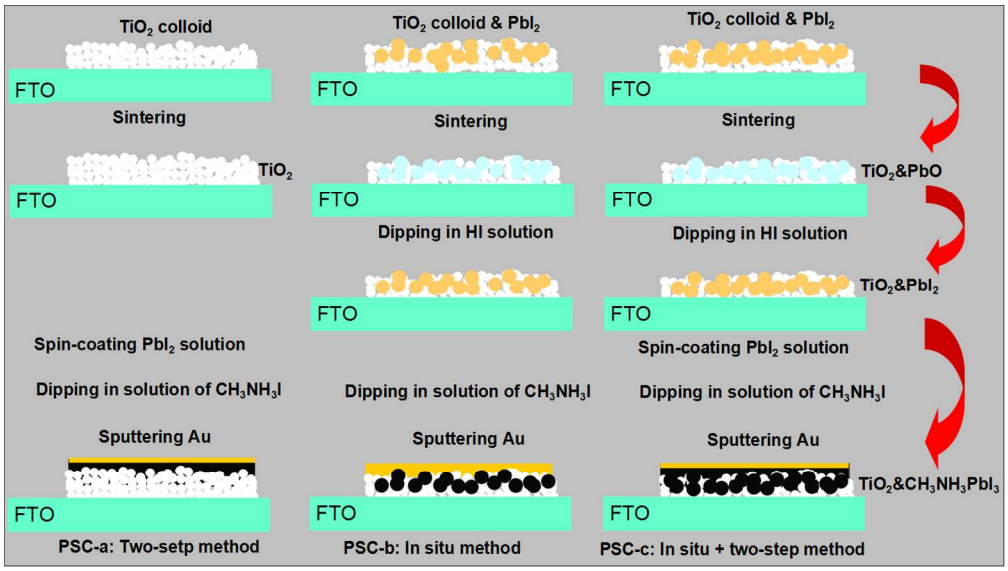

Figure 1 Schematic diagram of preparation processes for the three kinds of PSCs prepared by two-step, in situ, and in situ with two-step methods, respectively.
414x232mm (96 x 96 DPI)

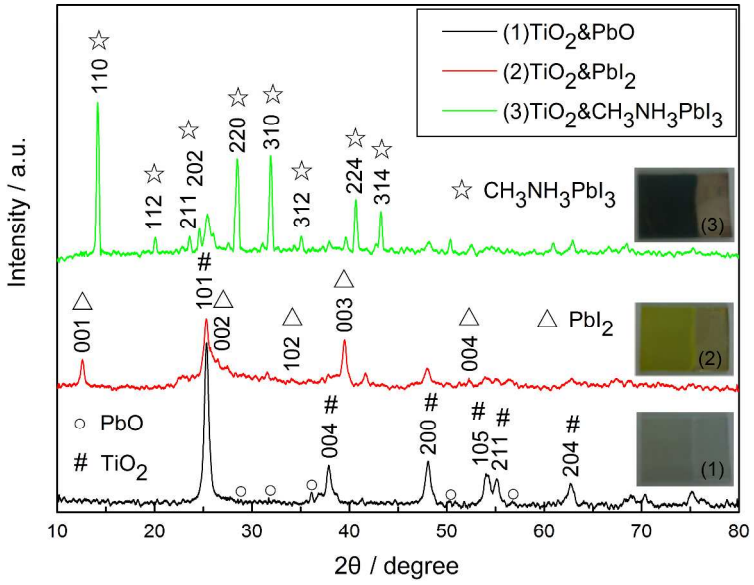

Figure 2 XRD patterns of the products in the in situ preparation process; Inset is the real photographs of the three products.
1187x839mm (150 x 150 DPI)

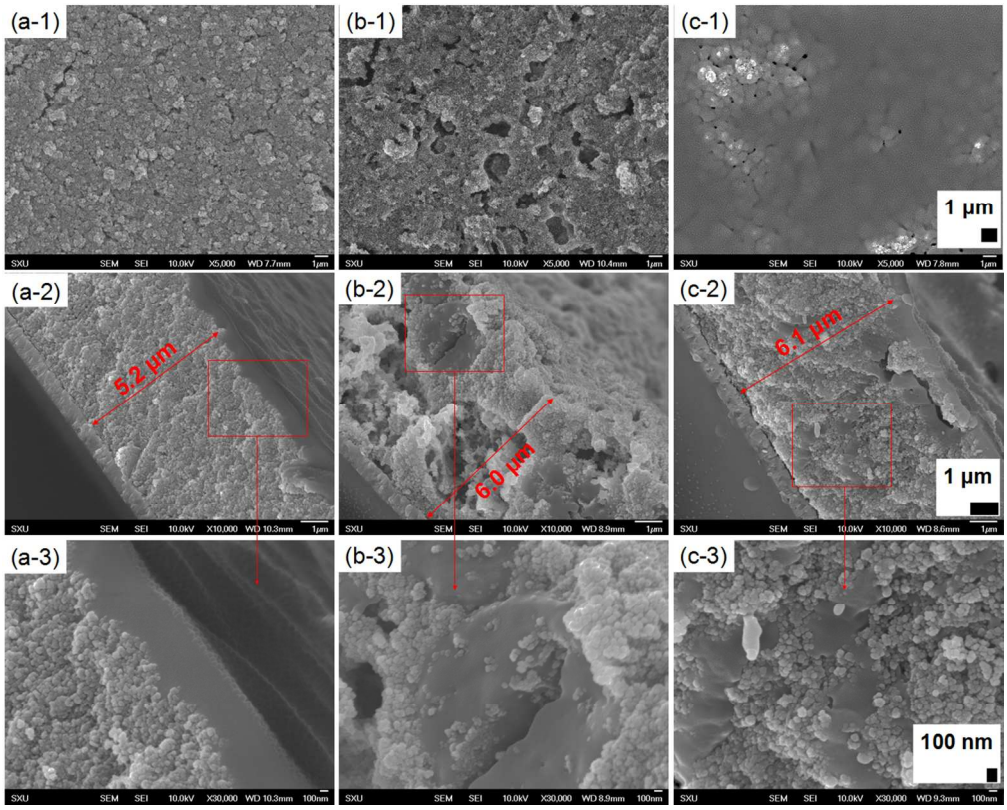

Figure 3 Top-view SEM images of the photoanodes by (a-1) two-step, (b-1) in situ, and (c-1) in situ with two-step methods, respectively; Cross-sectional SEM images of the photoanodes by (a-2, a-3) two-step, (b-2, b-3) in situ, and (c-2, c-3) in situ with two-step methods, respectively.
364x291mm (96 x 96 DPI)

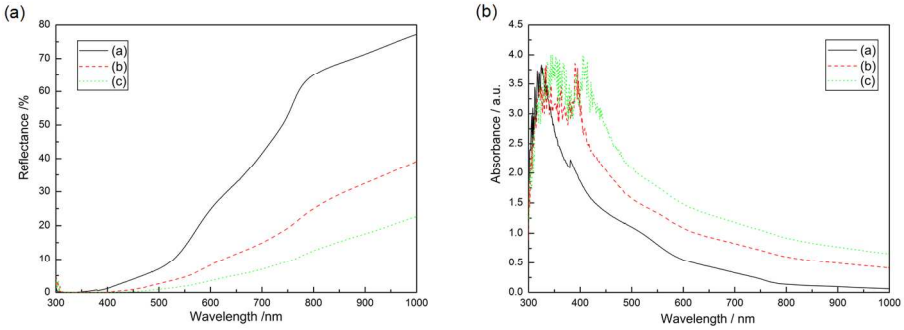

Figure 4 UV-Vis (a) Reflectance and (b) Adsorption spectra of the photoanodes by two-step, in situ, and in situ with two-step methods, respectively.
481x179mm (96 x 96 DPI)

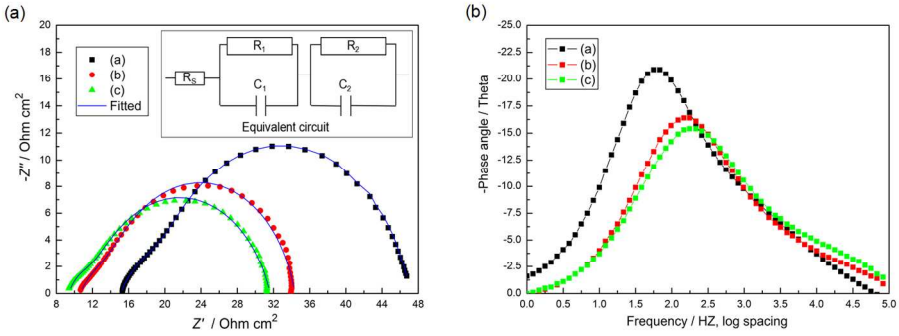

Figure 5 (a) Nyquist plots and (b) Bode phase plots of the PSC-a, PSC-b, and PSC-c, respectively; Inset (a) is the equivalent circuit of the PSC.
479x179mm (96 x 96 DPI)

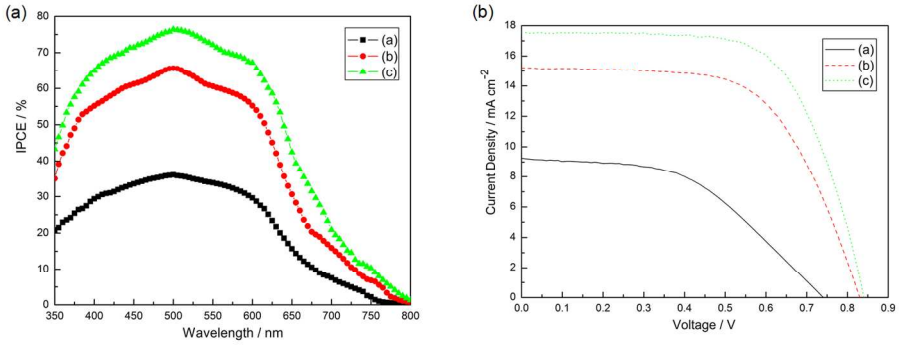

Figure 6 (a) IPCE and (b) Photocurrent density-voltage characteristics of the PSC-a, PSC-b, and PSC-c, respectively.
473x190mm (96 x 96 DPI)

Graphic Abstract

High performance perovskite-sensitized nanoporous titanium dioxide photoanodes by in situ method for use in perovskite solar cells

Yaoming Xiao*, Gaoyi Han*, Yanping Li, Miaoyu Li and Yunzhen Chang

Perovskite-sensitized nanoporous TiO_2 photoanode is firstly prepared by an in situ technique. The excellent contacting between the TiO_2 and perovskite could be beneficial to the separation and transmission of the electron and hole, the sufficient filling and abundant $CH_3NH_3PbI_3$ can enhance the absorption and utilization of sunlight, finally obtaining an efficient perovskite solar cell.

Keywords: in situ method, perovskite, titanium dioxide, photoanode, solar cell